Widely tunable second harmonic amplification by noncollinear phase matching in bulk birefringent materials

Devin J. Dean, Noah Flemens, Dylan Heberle, and Jeffrey Moses

School of Applied and Engineering Physics, Cornell University, Ithaca, New York 14853, USA

ABSTRACT

Second harmonic amplification — a hybridization of optical parametric amplification and second harmonic generation — is a route to ultra-efficient parametric amplification. Requiring the simultaneous phase matching of two parametric wave-mixing processes, it has limited frequency coverage in the collinear geometry in bulk media. Here we show that noncollinear birefringent phase matching can provide wide frequency tunability of second harmonic amplification across the near- and mid-infrared in the materials $ZnGeP_2$, $CdSiP_2$, $LiNbO_3$, $\beta-BaB_2O_4$, and KD_2PO_4 in applications designed for accommodating high-energy picosecond pulses generated by solid state lasers. We discuss practical limitations including acceptance angle, phase-matching bandwidth, spatial walk off, and parasitic processes.

Keywords: Second harmonic amplification, Noncollinear optical parametric amplification, Efficient picosecond pulse amplification, Back-conversion suppression, Idler second harmonic generation, Near-infrared generation, Mid-infrared generation

1. INTRODUCTION

Optical parametric amplification (OPA) is used to extend the frequency range of modern ultrafast laser systems and is commonly implemented in bulk birefringent media, allowing wide crystal apertures for high peak power and high average power applications.[1–5] However, conventional OPA schemes suffer from inherently low conversion efficiencies due to spatiotemporally inhomogeneous back-conversion.[6–8] Two types of approaches have been proposed, and in a few cases implemented, to combat the problem. One approach is to homogenize the conversion back-conversion cycle as best as possible, using flattop or conformal profiling techniques.[7–12] This is not a widespread solution due to the difficulty of shaping the pump and seed profiles without incurring significant losses in the process. Another homogenization method uses the passive pump pulse reshaping caused by spatiotemporal variations in impedance matching within an enhancement cavity.[13,14]

The other approach is to use back-conversion suppression.[15] Adiabatic frequency conversion,[16] which uses the nonlinear optical analog of rapid adiabatic passage via a swept phase-matching condition, is one such method. However, while adiabatic frequency conversion can achieve full photon population inversions in the presence of a strong wave in sum- and difference-frequency generation and four-wave mixing Bragg scattering,[17–20] in OPA, where the aim is to deplete the strong pump wave, there is still a bandwidth-efficiency trade-off.[16,21,22] Thus, while efficiency gains have been observed in adiabatic OPA processes, the technique is used more widely to extend bandwidth.[23–29]

Another method for back-conversion suppression is the use of loss at the idler wavelength to prevent signal-idler recombination. First proposed and demonstrated using linear loss, the technique has been used to achieve 40% conversion to the signal.[30–34] Recently we proposed the fully nonlinear, fully conservative process of second harmonic amplification (SHA) — a hybridization of OPA and idler second harmonic generation (SHG) — as an alternative route to achieving ultra-efficient parametric amplification and frequency conversion by prevention of signal-idler recombination.[35] Though the four-wave system is Hermitian (closed and loss-free), it possesses the dynamics of a non-Hermitian system due to the idler SHG process mimicking photon loss to a heat bath, with

Further author information:
D.J.D.: E-mail: dd482@cornell.edu

Nonlinear Frequency Generation and Conversion: Materials and Devices XX, edited by Peter G. Schunemann, Kenneth L. Schepler, Proc. of SPIE Vol. 11670, 116700G
 · doi: 10.1117/12.2584661

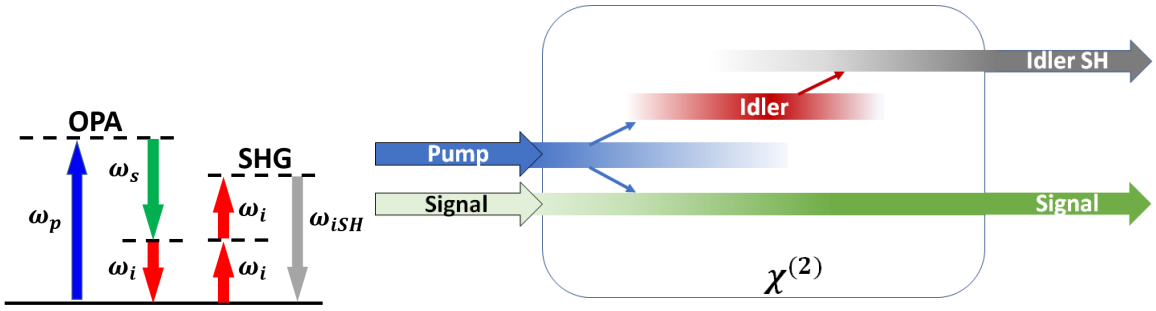

(a) (b)

Figure 1: Second Harmonic Amplification. (a) SHA Photon Exchange Diagram. In OPA, photons at the pump frequency are annihilated when interacting with the nonlinear crystal's polarization field, creating equal photon numbers at the signal and idler frequencies. Simultaneously, in the SHG process pairs of photons from the idler field are annihilated while generating photons at double the idler's frequency. (b) SHA Schematic. A strong pump and weak signal are input to a second order nonlinear crystal and through SHA the signal and idler's second harmonic are amplified.

unidirectional flow of photons to the idler second harmonic (SH).[36] The dynamics of SHA are damped conversion back-conversion cycles that allow nearly all spatiotemporal coordinates to achieve full pump depletion at the same crystal length, thus avoiding the inhomogeneous spatiotemporal back-conversion that limits the efficiency of most OPA devices. The resulting pump-to-signal conversion efficiencies of over 50%, with most of the remaining power in the idler SH wave.[35]

The energy exchange of SHA is depicted in Fig. 1. As shown, SHA requires the simultaneous phase matching of both OPA and SHG of the idler beam. In other words, SHA occurs when the phase mismatch of OPA and idler SHG are both zero:

$$\Delta \boldsymbol{k}_{OPA} = \boldsymbol{k}_p - \boldsymbol{k}_s - \boldsymbol{k}_i = 0, \tag{1}$$

and

$$\Delta \boldsymbol{k}_{SHG} = \boldsymbol{k}_{iSH} - 2\boldsymbol{k}_i = 0. \tag{2}$$

Birefringent phase matching in a collinear geometry and quasi-phase matching of SHA have been investigated in prior work. In these approaches, the simultaneous phase matching of OPA and idler SHG occurs only at a specific signal wavelength for any given pump wavelength.[35] In this work, we investigate noncollinear SHA in bulk media to enable broad tunability and high power applications. We note that while a wide body of literature has investigated hybridized parametric processes,[37] including works specifically investigating simultaneous phase matching of OPA and SHG, *e.g.*,[38–40] here we address the problem in the context of high efficiency frequency conversion by SHA and the associated limiting factors of the noncollinear application in bulk materials. We show that type-I noncollinear birefringent phase matching can be used for wide frequency tuning of SHA across the near- and mid-infrared in various nonlinear crystals, including $ZnGeP_2$, $CdSiP_2$, $LiNbO_3$, $\beta - BaB_2O_4$, and KD_2PO_4. We also discuss practical limitations such as acceptance angle, phase-matching bandwidth, and gain competition between SHA, conventional OPA, and two parasitic processes. Through its use of low-loss bulk nonlinear media, noncollinear SHA may provide a general solution for efficient and tunable amplification with high-energy picosecond laser beams.

2. NONCOLLINEAR BIREFRINGENT SECOND HARMONIC AMPLIFICATION

It is desirable for an amplifier to be tunable, i.e., to provide flexible choice of signal wavelength for a given pump wavelength. SHA is not tunable when all beams are collinear. For a fixed set of wavelengths, idler SHG is phase matched at one crystal orientation and collinear OPA is phase matched at another. If these angles are not the same, collinear SHA is not possible for that set of wavelengths.

Our proposed route to tunability uses a noncollinear geometry. While noncollinear phase matching is widely used to extend the phase-matching bandwidth of OPAs to the few-cycle regime,[1] in which the angle between

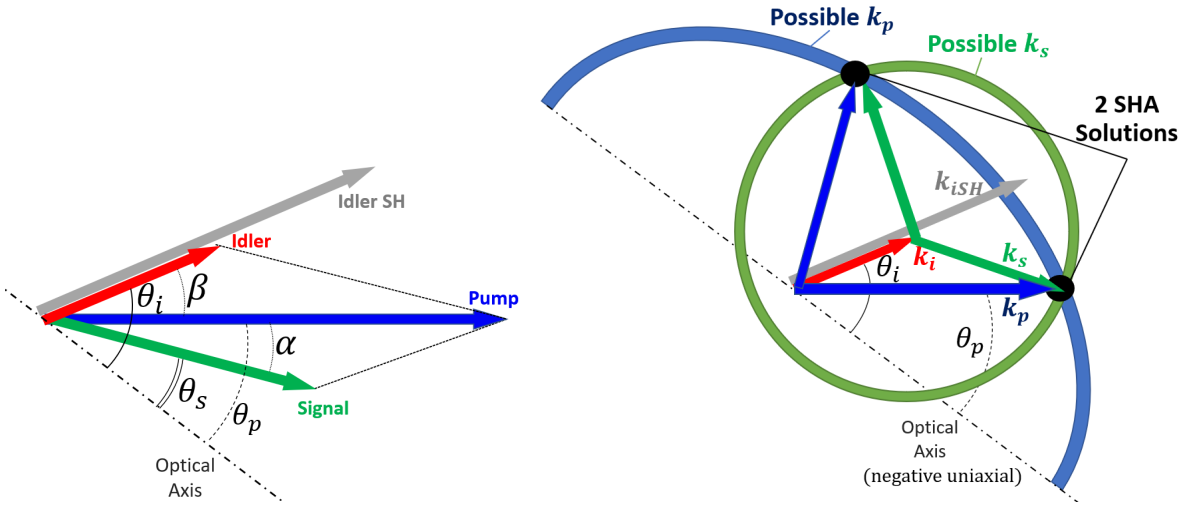

(a) (b)

Figure 2: (a) Wave-vector diagram for noncollinear SHA. We can either refer to the beams by their propagation with respect to the optical axis θ or by their propagation relative to the pump (α for the signal and β for the idler SH. (b) Illustration of why noncollinear SHA typically has either 0 or 2 solutions for a given set of wavelengths, allowing for tunability. This diagram sketches the phase matching in a negative uniaxial crystal, so the idler SH and pump lie on the extraordinary axis. There is only one angle that phase matches idler SHG, so the idler wave vector is fixed. The signal wave vector has fixed length but can point in any direction (green circle of possibilities). The pump wave vector varies with angle (blue ellipse), leading to two points where the sum of idler and signal wave vectors equal the pump's - that is, where OPA and idler SHG are simultaneously phase matched, and the process of SHA can occur.

pump and seed beams provides an additional degree of freedom for achieving their group-velocity matching, here we use the new degree of freedom to satisfy the dual phase matching of OPA and SHG for signal wavelengths in a given nonlinear medium with a given pump wavelength. The noncollinear geometry is shown in Fig. 2a. Assuming idler photons are generated with a single polarization, idler SHG is necessarily a type-I process. The OPA could be either type-I or type-II. In this paper we only consider type-I phase matching in birefringent uniaxial crystals and find that this offers a wide tuning range. Our diagrams show the case of negative uniaxial crystals, but can be extended to positive uniaxial crystals.

Figure 2b illustrates how noncollinearity allows for dual phase matching. Idler SHG is phase matched at one angle for a given signal wavelength, so the magnitude and direction of the idler wave vector are fixed. The signal wave vector has fixed length, but it can point in any direction in a noncollinear setup. If we superimpose all possible pump angles, we see that there can be up to two points where simultaneous phase matching of OPA and idler SHG is possible for a given set of pump and signal wavelengths. In general, noncollinear SHA can have up to 2 solutions, so we label the solution that has the pump at a smaller θ as solution 1.

To visualize the SHA solutions for a fixed pump wavelength, we plot the tuning curves of propagation angle θ vs signal wavelength. Figure 3 is the SHA tuning curve in lithium niobate ($LiNbO_3$) pumped at 1030 nm. Since idler SHG only occurs at one angle for a given wavelength set, we can plot the idler tuning curve (red line). Any OPA tuning curves that have the idler propagate along this red line are SHA solutions and are also plotted (solution 1 is solid and 2 is dashed). For this particular case, the only collinear solution is at degeneracy ($\lambda_s = \lambda_i = 2.06\ \mu m$), but with other pump wavelengths or other crystals the tuning curve differs and can have two collinear solutions. At degeneracy, SHA is equivalent to OPA alone, and there will always be one collinear solution.

2.1 ANGULAR ACCEPTANCE AND BANDWIDTH TOLERANCE

SHA requires phase matching over the entire bandwidth and angular spread of the beams for both the OPA and SHG processes for efficient conversion. Otherwise, some portion of the OPA process will experience back-

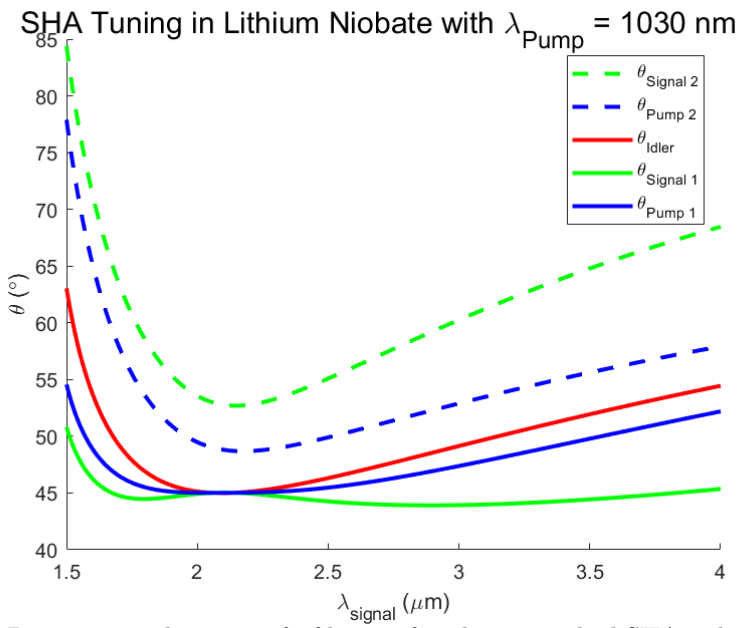

Figure 3: SHA Tuning: Propagation directions θ of beams for phase matched SHA in lithium niobate pumped at 1030 nm. In red is the (only) idler tuning curve, and in solid and dashed lines are two possible pump and signal tuning curves. The difference in direction between the pump (blue) and signal (green) is the signal noncollinear angle α.

conversion, and the problem of spatiotemopral conversion inhomogeneity will persist. We use the heuristic that SHA occurs most efficiently when $f(\lambda_s, \theta_p, \theta_s) = (\Delta \boldsymbol{k}_{OPA}^2 + \Delta \boldsymbol{k}_{SHG}^2)^{1/2}$ is minimized. While previous work has shown SHA efficiency depends on the relative signs of $\Delta \boldsymbol{k}_{OPA}$ and $\Delta \boldsymbol{k}_{SHG}$,[35] we find this to be a suitable condition for optimizing the process. Figure 3 showed all points λ_s, θ_p, θ_s, and θ_i where $f(\lambda_s, \theta_p, \theta_s) = 0$. For perfect phase matching there is a direct relation between signal and idler directions, but the relation is not obvious for $f(\lambda_s, \theta_p, \theta_s) \neq 0$. In normal OPA, the idler propagates at an angle that minimizes $\Delta \boldsymbol{k}_{OPA}$.[41] For SHA, where the first process that occurs is OPA, the idler still appears in the direction that minimizes $\Delta \boldsymbol{k}_{OPA}$.

To determine the SHA acceptance bandwidth and angular divergence, we plot a surface of constant $f(\lambda_s, \theta_p, \theta_s)$ superimposed on boxes representing ranges in our parameter space. The length of the box along λ_s, θ_p, and θ_s corresponds to the signal bandwidth, pump divergence, and signal divergence respectively. The constant value of $f(\lambda_s, \theta_p, \theta_s)$ was chosen according to collinear simulations[35] as 0.1 mm^{-1}. Locations where the box protrudes from the constant surface of $f(\lambda_s, \theta_p, \theta_s)$ violates our phase matching constraint. Figures 4a, 4b, and 4c depict the surfaces of $f(\lambda_s, \theta, \alpha) = 0.1\ mm^{-1}$ and the boxes in parameter space that correspond to different experimental parameters for SHA in lithium niobate pumped at 1.03 μm with a signal wavelength of about 1.88 μm. It is desirable for most of the box to lie within the surface, as this implies that a large portion of the beams will simultaneously have low phase mismatch of OPA and SHG.

There are two possible routes to better phase matching at a given wavelength: decreasing the beam divergences or decreasing the signal bandwidth. The roughly doubled beam sizes in Fig. 4b result in much more of the parameter space being phase matched compared to that of Fig. 4a - so we see that the angular-acceptance constraint strongly favors large beam sizes. Figures 4a and 4c depict parameter-boxes corresponding to beams of equal size but with bandwidths of 3-ps and 10-ps transform-limited pulses, respectively. The phase matching is only slightly better for the 10-ps pulse. Though the amplification bandwidth depends on the particular set of wavelengths and beam sizes, the bandwidth tolerance of SHA is theoretically broad enough to amplify picosecond pulses.

The relative phase-matching bandwidth can be inferred from the tuning curve: the smaller the slope of all of the beam propagation angles, the larger the bandwidth that can be phase matched for a given set of propagation

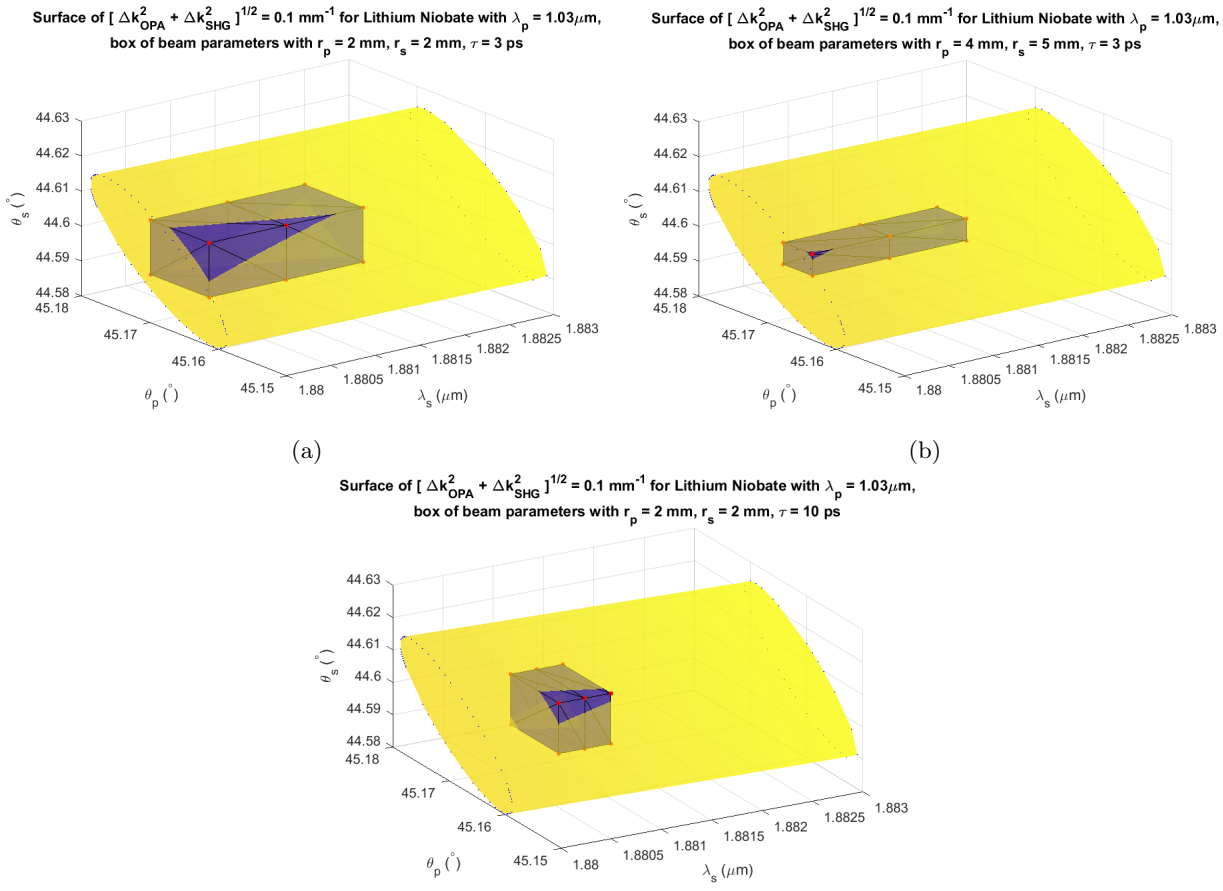

(a) (b)

(c)

Figure 4: Surfaces of $f(\lambda_s, \theta, \alpha) = 0.1\ mm^{-1}$, with superimposed box representing the space of desired beam parameters. (a) Beam parameters determined by: $r_p = r_s = 2$ mm ($1/e^2$ max) and the bandwidth of a $\tau = 3$ ps pulse (FWHM) at $\lambda_s = 1.88\ \mu m$. (b) Beam parameters determined by: $r_p = 4$ mm, $r_s = 5$ mm and duration $\tau = 3$ ps. (c) Beam parameters determined by: $r_p = r_s = 2$ mm and duration $\tau = 10$ ps.

angles. For example, in Fig. 3 we see the phase-matching bandwidth is largest near degeneracy. However, as we discuss in section 2.3, we must avoid wavelengths too close to degeneracy due to parasitic processes that are phase matched at degeneracy.

2.2 SPATIAL WALK OFF

In SHA, the usual OPA interaction length limitations due to temporal and spatial walk off are complicated by the presence of four beams. As usual, temporal walk off is the effect of group-velocity mismatch, which is generally negligible for picosecond pulses in the sub-centimeter devices considered here. Spatial walk off can occur either when a beam's wave vector is not parallel to the pump's wave vector (noncollinear walk off) or when the beam is polarized along the extraordinary axis and induces Poynting vector walk off. The beams' propagation directions in SHA (ignoring divergence) are outlined in Table 1 for a negative uniaxial crystal. In conventional OPA, a "walk off compensating" configuration, where the Poynting vectors of the extraordinarily polarized waves walk toward the propagation direction of the other waves, can be employed to increase the interaction length. SHA, however, requires significant interaction between all four beams and the notion of walk off compensation doesn't apply. Previous work found, for a specific crystal and set of wavelengths, that an estimate for the maximum allowable separation of beams in SHA is one tenth of the pump's radius. Larger separations resulted in back-conversion oscillations that lowered the conversion efficiency.[35] Generally, we find that beams of a few mm in

Beam	Noncollinear walk off	Poynting walk off	Total walk off
λ_p	0 by definition	ρ_p	ρ_p
λ_s	$-\alpha$	0	$-\alpha$
λ_i	β	0	β
λ_{iSH}	β	ρ_{iSH}	$\beta + \rho_{iSH}$

Table 1: Contributions to total walk off in SHA with respect to the wave vector of the pump $\boldsymbol{k}_p$ in a negative uniaxial crystal.

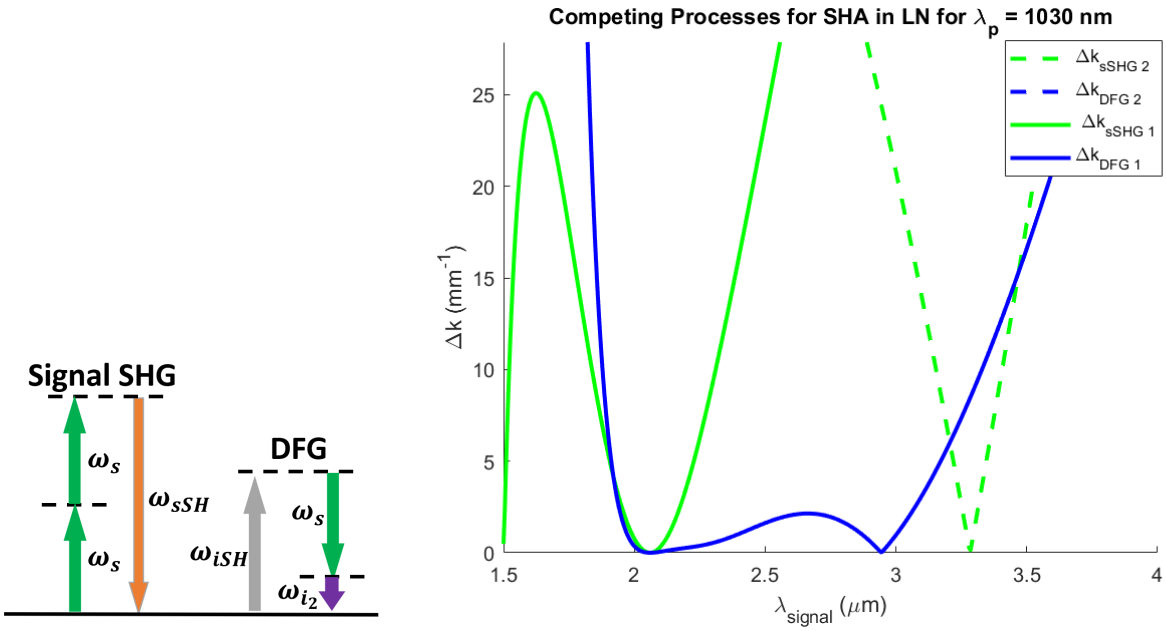

(a) (b)

Figure 5: Parasitic processes. (a) Photon exchange diagram of the nonlinear processes signal SHG and DFG between the idler SH and signal. (b) Phase mismatch of these two parasitic processes calculated for points along the lithium niobate SHA tuning curve shown in Fig. 3. Note that at degeneracy (when $\omega_s = \omega_i$), both of these processes are phase matched for one of the SHA solutions.

radius are not quite large enough to mitigate the effects of spatial walk off for signal noncollinear walk off greater than $\sim 4°$.

2.3 PARASITIC PROCESSES

There are two other parametric processes that must be accounted for when considering the tuning range of SHA: signal SHG and difference frequency generation (DFG) between the idler SH and signal. The energy diagram for these processes is shown in Fig. 5a. It is important to note that both of these processes are perfectly phase matched at the degenerate SHA solution (when $\omega_s = \omega_i$), so they are close to being phase matched for wavelengths near degeneracy. These processes are parasitic because they can introduce oscillations that disturb the damped oscillatory conversion of SHA leading to back-conversion and lowering conversion efficiencies. Furthermore, signal SHG removes energy from the signal that we wish to amplify.

Figure 5b displays the phase mismatch of the parasitic processes for the SHA solutions in lithium niobate pumped by 1030 nm as shown in Fig. 3. If we consider the minimum acceptable phase mismatch of the parasitic processes to be 4 mm^{-1} (estimated from collinear simulations), then solution 1 is not limited by parasitic DFG or signal SHG over the wavelength ranges 1.5 - 1.91 μm and 3.135 - 4 μm. Solution 2 (dashed) is largely unimpeded by these parasitic processes - however, it requires noncollinear angles in excess of $\alpha = 4°$, which imposes its limitations through spatial walk off, discussed in Sec. 2.2.

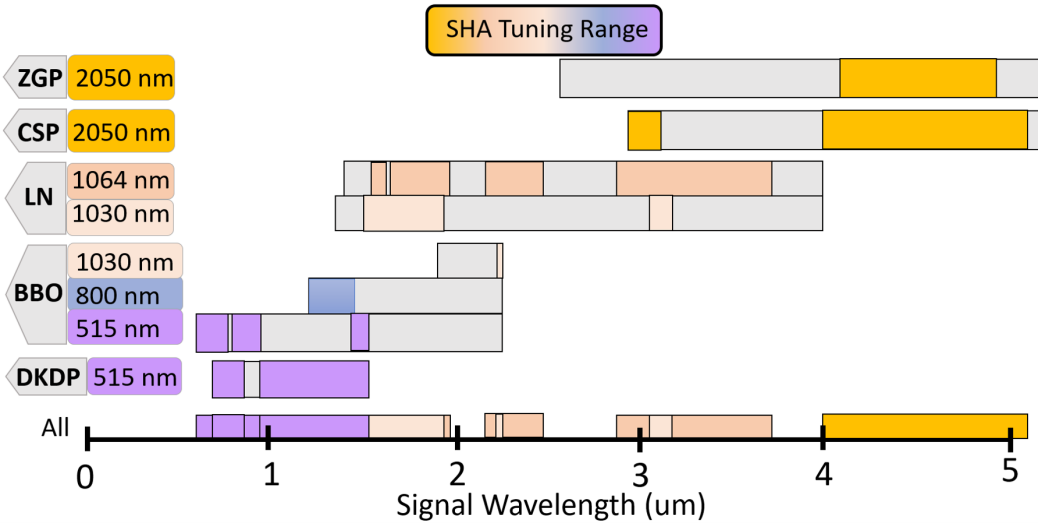

Figure 6: Approximate feasible tuning range in various nonlinear crystals pumped by common high-power picosecond laser systems. Gray: Conventional OPA tuning range (limited by transparency window for 80% transmission after 1 cm propagation). Colored by pump wavelength (on top of gray): Feasible SHA tuning range, accounting for spatial walkoff ($\alpha < 4°$) and parasitic processes ($\Delta k_{sSHG} > 4\ mm^{-1}$, $\Delta k_{DFG} > 4\ mm^{-1}$).

3. FEASIBLE TUNING RANGE

We estimate the portion of the near- to mid-IR that can be amplified with SHA by considering its limitations in important OPA crystals pumped by various common pump wavelengths. To get an approximate tuning range of SHA, we exclude solutions that have either large walk off signified by $\alpha > 4°$ or well phase matched parasitic processes signified by $\Delta k_{sSHG} < 4\ mm^{-1}$ and $\Delta k_{DFG} < 4\ mm^{-1}$.

Figure 6 displays the tuning range of SHA superimposed on that of conventional OPA in the nonlinear crystals $ZnGeP_2$ (ZGP), $CdSiP_2$ (CSP), $LiNbO_3$ (LN), $\beta - BaB_2O_4$ (BBO), and KD_2PO_4 (DKDP). The displayed pump wavelengths were chosen based on existing high-power picosecond laser sources: Ho:YLF at 2050 nm, Nd:YAG at 1064 nm, Yb:YAG at 1030 and 515 nm, and Ti:Sapphire at 800 nm. Some portions of the tuning range have two viable SHA solutions for a given crystal, pump, and signal wavelength, but the majority only have one. The figure illustrates that noncollinear SHA is feasible across about 75% of the range from 0.7 - 5 μm. These tuning ranges are estimates based on the analysis above; numerical simulations of the noncollinear interaction would define them more precisely.

4. CONCLUSIONS AND FUTURE WORK

We have shown that SHA, requiring the simultaneous phase matching of OPA and idler SHG, is widely tunable with noncollinear birefringent phase matching in uniaxial crystals. After considering constraints imposed by angular and bandwidth acceptance, spatial walk off and coincidental phase matching of two parasitic processes, we concluded that noncollinear SHA is feasible across much of the $0.7 - 5\ \mu m$ range when paired with common high-power picosecond laser systems. This implies that SHA is a possible avenue to tunable, high-efficiency, high-energy frequency conversion for many applications.

ACKNOWLEDGMENTS

This work was partially supported by the NSF via ECCS-1944653 and by the Cornell Center for Materials Research with funding from the NSF MRSEC program (DMR-1719875).

REFERENCES

[1] Cerullo, G. and De Silvestri, S., "Ultrafast optical parametric amplifiers," *Rev. Sci. Instrum.* **74**(1), 1–18 (2003).

[2] Mourou, G. A., Tajima, T., and Bulanov, S. V., "Optics in the relativistic regime," *Rev. Mod. Phys.* **78**, 309–371 (Apr 2006).

[3] Dubietis, A., Butkus, R., and Piskarskas, A. P., "Trends in chirped pulse optical parametric amplification," *IEEE J. Sel. Top. Quantum Electron.* **12**(2), 163–172 (2006).

[4] Witte, S. and Eikema, K. S. E., "Ultrafast optical parametric chirped-pulse amplification," *IEEE J. Sel. Top. Quantum Electron.* **18**(1), 296–307 (2012).

[5] Fattahi, H., Barros, H. G., Gorjan, M., Nubbemeyer, T., Alsaif, B., Teisset, C. Y., Schultze, M., Prinz, S., Haefner, M., Ueffing, M., Alismail, A., Vámos, L., Schwarz, A., Pronin, O., Brons, J., Geng, X. T., Arisholm, G., Ciappina, M., Yakovlev, V. S., Kim, D.-E., Azzeer, A. M., Karpowicz, N., Sutter, D., Major, Z., Metzger, T., and Krausz, F., "Third-generation femtosecond technology," *Optica* **1**, 45–63 (Jul 2014).

[6] Mironov, G. V. and Filonenko, N. N., "Optical inhomogeneity of nonlinear crystals and maximum efficiencies of parametric frequency amplifiers pumped by beams with inhomogeneous transverse intensity distributions," *Sov. J. Quantum Electron.* **12**, 723–727 (jun 1982).

[7] Begishev, I. A., Gulamov, A. A., Erofeev, E. A., Ibragimov, É. A., Kamalov, S. R., Usmanov, T., and Khadzhaev, A. D., "Highly efficient parametric amplification of optical beams. i. optimization of the profiles of interacting waves in parametric amplification," *Sov. J. Quantum Electron.* **20**, 1100–1103 (sep 1990).

[8] Moses, J. and Huang, S.-W., "Conformal profile theory for performance scaling of ultrabroadband optical parametric chirped pulse amplification," *J. Opt. Soc. Am. B* **28**, 812–831 (2011).

[9] Bagnoud, V., Begishev, I., Guardalben, M., Puth, J., and Zuegel, J., "5 hz, >250 mj optical parametric chirped-pulse amplifier at 1053 nm," *Opt. Lett.* **30**, 1843–1845 (2005).

[10] Fülöp, J. A., Major, Z., Horváth, B., Tavella, F., Baltuška, A., and Krausz, F., "Shaping of picosecond pulses for pumping optical parametric amplification," *Appl. Phys. B* **87**, 79–84 (2007).

[11] Cao, H., Tóth, S., Kalashnikov, M., Chvykov, V., and Osvay, K., "Highly efficient, cascaded extraction optical parametric amplifier," *Opt Express* **26**, 7516–7527 (2018).

[12] Fischer, P., Muschet, A., Lang, T., Salh, R., and Veisz, L., "Saturation control of an optical parametric chirped-pulse amplifier," *Opt. Express* **29**, 4210–4218 (Feb 2021).

[13] Siddiqui, A. M., Moses, J., Hong, K.-H., Lai, C.-J., and Kärtner, F. X., "Performance scaling via passive pulse shaping in cavity-enhanced optical parametric chirped-pulse amplification," *Opt. Lett.* **35**, 1929–1931 (Jun 2010).

[14] Siddiqui, A. M., Hong, K.-H., Moses, J., and Kärtner, F. X., "Bandwidth extension and conversion efficiency improvements beyond phase matching limitations using cavity-enhanced opcpa," *Opt. Express* **29**, 9907–9926 (Mar 2021).

[15] Moses, J., Flemens, N., and Ding, X., "Back-conversion suppressed parametric frequency conversion for ultrawide bandwidth and ultrahigh efficiency devices," in [*Nonlinear Frequency Generation and Conversion: Materials and Devices XIX*], Schunemann, P. G. and Schepler, K. L., eds., **11264**, 41 – 51, International Society for Optics and Photonics, SPIE (2020).

[16] Suchowski, H., Porat, G., and Arie, A., "Adiabatic processes in frequency conversion," *Laser & Photonics Rev.* **8**(3), 333–367 (2014).

[17] Suchowski, H., Oron, D., Arie, A., and Silberberg, Y., "Geometrical representation of sum frequency generation and adiabatic frequency conversion," *Phys. Rev. A* **78**(6), 063821 (2008).

[18] Moses, J., Suchowski, H., and Kärtner, F. X., "Fully efficient adiabatic frequency conversion of broadband ti: sapphire oscillator pulses," *Opt. Lett.* **37**(9), 1589–1591 (2012).

[19] Bahar, E., Ding, X., Dahan, A., Suchowski, H., and Moses, J., "Adiabatic four-wave mixing frequency conversion," *Opt. Express* **26**(20), 25582–25601 (2018).

[20] Ding, X., Heberle, D., Harrington, K., Flemens, N., Chang, W.-Z., Birks, T. A., and Moses, J., "Observation of rapid adiabatic passage in optical four-wave mixing," *Phys. Rev. Lett.* **124**, 153902 (Apr 2020).

[21] Phillips, C. R. and Fejer, M. M., "Efficiency and phase of optical parametric amplification in chirped quasi-phase-matched gratings," *Opt. Lett.* **35**, 3093–3095 (Sep 2010).

[22] Porat, G. and Arie, A., "Efficient, broadband, and robust frequency conversion by fully nonlinear adiabatic three-wave mixing," *J. Opt. Soc. Am. B* **30**(5), 1342–1351 (2013).
[23] Charbonneau-Lefort, M., Afeyan, B., and Fejer, M. M., "Optical parametric amplifiers using chirped quasi-phase-matching gratings i: practical design formulas," *J. Opt. Soc. Am. B* **25**, 463–480 (Apr 2008).
[24] Heese, C., Phillips, C. R., Gallmann, L., Fejer, M. M., and Keller, U., "Ultrabroadband, highly flexible amplifier for ultrashort midinfrared laser pulses based on aperiodically poled mg:linbo3," *Opt. Lett.* **35**, 2340–2342 (Jul 2010).
[25] Heese, C., Phillips, C. R., Mayer, B. W., Gallmann, L., Fejer, M. M., and Keller, U., "75 mw few-cycle mid-infrared pulses from a collinear apodized appln-based opcpa," *Opt. Express* **20**, 26888–26894 (Nov 2012).
[26] Mayer, B. W., Phillips, C. R., Gallmann, L., and Keller, U., "Mid-infrared pulse generation via achromatic quasi-phase-matched opcpa," *Opt Express* **22**, 20798–20808 (2014).
[27] Markov, A., Mazhorova, A., Breitenborn, H., Bruhacs, A., Clerici, M., Modotto, D., Jedrkiewicz, O., di Trapani, P., Major, A., Vidal, F., and Morandotti, R., "Broadband and efficient adiabatic three-wave-mixing in a temperature-controlled bulk crystal," *Opt. Express* **26**, 4448–4458 (Feb 2018).
[28] Rozenberg, E. and Arie, A., "Broadband and robust adiabatic second-harmonic generation by a temperature gradient in birefringently phase-matched lithium triborate crystal," *Opt. Lett.* **44**, 3358–3361 (Jul 2019).
[29] Margules, P., Moses, J., Suchowski, H., and Porat, G., "Ultrafast adiabatic frequency conversion," *Journal of Physics: Photonics* (2021).
[30] Ma, J., Wang, J., Yuan, P., Xie, G., Xiong, K., Tu, Y., Tu, X., Shi, E., Zheng, Y., and Qian, L., "Quasi-parametric amplification of chirped pulses based on a sm3+-doped yttrium calcium oxyborate crystal," *Optica* **2**, 1006–1009 (Nov 2015).
[31] El-Ganainy, R., Dadap, J. I., and Osgood, R. M., "Optical parametric amplification via non-hermitian phase matching," *Opt. Lett.* **40**, 5086–5089 (Nov 2015).
[32] Zhong, Q., Ahmed, A., Dadap, J. I., Osgood, R. M., and El-Ganainy, R., "Parametric amplification in quasi-pt symmetric coupled waveguide structures," *New J. Phys.* **18**, 125006 (2016).
[33] Ma, J., Wang, J., Zhou, B., Yuan, P., Xie, G., Xiong, K., Zheng, Y., Zhu, H., and Qian, L., "Broadband, efficient, and robust quasi-parametric chirped-pulse amplification," *Opt. Express* **25**, 25149–25164 (Oct 2017).
[34] Yin, Z., Ma, J., Wang, J., Yuan, P., Xie, G., and Qian, L., "Quasi-parametric chirped-pulse amplification simultaneously enables high peak power and high average power," *IEEE Photonics Journal* **11**(4), 1–12 (2019).
[35] Flemens, N., Swenson, N., and Moses, J., "Second harmonic amplification," in [*OSA Advanced Photonics Congress (AP) 2020 (IPR, NP, NOMA, Networks, PVLED, PSC, SPPCom, SOF)*], *OSA Advanced Photonics Congress (AP) 2020 (IPR, NP, NOMA, Networks, PVLED, PSC, SPPCom, SOF)* , NpM4D.6, Optical Society of America (2020).
[36] Flemens, N. and Moses, J., "Non-hermitian dynamics mimicked by a fully parametric hybrid nonlinear optical system," in [*OSA Advanced Photonics Congress (AP) 2020 (IPR, NP, NOMA, Networks, PVLED, PSC, SPPCom, SOF)*], *OSA Advanced Photonics Congress (AP) 2020 (IPR, NP, NOMA, Networks, PVLED, PSC, SPPCom, SOF)* , NpM3E.2, Optical Society of America (2020).
[37] Saltiel, S. M., Sukhorukov, A. A., and Kivshar, Y. S., "Chapter 1 - multistep parametric processes in nonlinear optics," *Progress in Optics* **47**, 1–73, Elsevier (2005).
[38] Lee, C.-K., Zhang, J.-Y., Huang, J. Y., and Pan, C.-L., "Generation of femtosecond laser pulses tunable from 380 nm to 465 nm via cascaded nonlinear optical mixing in a noncollinear optical parametric amplifier with a type-i phase matched bbo crystal," *Opt. Express* **11**, 1702–1708 (Jul 2003).
[39] Bromage, J., Rothhardt, J., Hädrich, S., Dorrer, C., Jocher, C., Demmler, S., Limpert, J., Tünnermann, A., and Zuegel, J. D., "Analysis and suppression of parasitic processes in noncollinear optical parametric amplifiers," *Opt. Express* **19**, 16797–16808 (Aug 2011).
[40] Aytur, O. and Dikmelik, Y., "Plane-wave theory of self-doubling optical parametric oscillators," *IEEE Journal of Quantum Electronics* **34**(3), 447–458 (1998).
[41] Zheng, J. and Zacharias, H., "Non-collinear optical parametric chirped-pulse amplifier for few-cycle pulses," *Applied Physics B* **97**, 765–779 (12 2009).